Computer Physics Communications 129 (2000) 233–246

Computer Physics Communications

www.elsevier.nl/locate/cpc

Numerical simulation of two- and three-dimensional two-phase fluid motion by lattice Boltzmann method

Naoki Takada [a,*], Masaki Misawa [a,1], Akio Tomiyama [b,2], Shinya Fujiwara [b,3]

[a] *Mechanical Engineering Laboratory, AIST, 1-2, Namiki, Tsukuba, Ibaraki 305-8564, Japan*

[b] *Department of Engineering, Kobe University, 1-1, Rokkodai-cho, Nada, Kobe 657-8501, Japan*

Abstract

This study describes the numerical simulations of two-phase fluid motions under gravity by the lattice Boltzmann method (LBM), in which the fluid motions result from collision and translation of mesoscopic particles and the interface interaction in multiphase fluids can be reproduced in a self-organizing way. Our aims are to examine the applicability of LBM to the numerical analysis of bubble motions in comparison with the two-dimensional results by the Volume Of Fluid (VOF) method based on the Navier–Stokes and the liquid-volume convective equations, and to develop the three-dimensional binary fluids model, consisting of two sets of distribution functions to represent the total fluid density and the density difference, which introduces the repulsive interaction consistent with a free energy function between fluid particles. We included the buoyancy terms due to the density difference between two phases in the lattice Boltzmann equations, and simulated the motions of single bubble and two bubbles rising in a duct, calculating the surface tension from the Laplace's law represented by the non-dimensional numbers, Eotvos and Morton numbers. In the two-dimensional simulations, the results by LBM agree with those by the VOF method. The three-dimensional simulation of two bubble interaction shows that the upper bubble takes a shape of skirt as the lower bubble approaches due to the wake formation, and they coalesce into a single bubble eventually. These results prove the validity of the buoyancy model proposed here and the applicability of LBM to the quantitative numerical analysis of two-phase fluid motions.

PACS: 47.55.K; 47.55.D; 47.32; 47.11

Keywords: Lattice Boltzmann method; Binary fluids model; Two-phase fluid; Volume of fluid method; Bubble; Surface tension

1. Introduction

The lattice Boltzmann method (LBM) has been proposed as a mesoscopic approach to the numerical simulations of fluid motions on the assumption that a fluid consists of many particles repeating collision and translation and distributions converge to a state of local equilibrium. LBM, based on the lattice gas cellular automaton [2,3], possesses some advantages such as relatively easy implementation of boundary conditions on complex geometries, high efficiency on parallel processing, and easy and flexible reproduction of interfaces between phases.

In LBM, several kinds of multiphase fluid model have already been developed and applied to some simulations of phase separation and transition. The first immiscible multiphase model [4,5] reproduced the

* Corresponding author. E-mail: mv249@mel.go.jp.

[1] E-mail: misawa@mel.go.jp.

[2] E-mail: tomiyama@mech.kobe-u.ac.jp.

[3] E-mail: fujiwara@mp-3.mech.kobe-u.ac.jp.

0010-4655/00/$ – see front matter
PII: S0010-4655(00)00110-7

phase separation by the repulsive interaction based on the color gradient and the color momentum between red- and blue-colored particles representing two kinds of fluid. Shan and Chen proposed the gas–liquid model applicable to the phase transition with the potential between particles [6,7], while another gas–liquid model proposed by Swift et al. [8] simulates phase transitions consistent with the thermodynamics on the theory of van der Waals–Cahn–Hillard free energy. However, LBM has hardly been applied to any quantitative numerical analysis of the motion of bubble or droplet in two-phase flows under gravity, particularly in three dimensions.

Therefore, in LBM, we consider the buoyancy effect due to density difference in two-phase fluid characterized with the non-dimensional numbers such as Eotvos and Morton numbers and develop the three-dimensional binary fluids model proposed by Swift et al. [9]. In this paper, we will show the numerical results of bubble motions, which are compared with the two-dimensional results by the Volume Of Fluid (VOF) method based on the finite difference of macroscopic hydrodynamic equations [10]. The numerical results by the 3D model are also presented. Hereafter, a low density phase is referred to as gas or bubble, and a high density phase as liquid, although these fluids do not correspond to actual fluids exactly because of the small density ratio.

We explain the binary fluids model in the next section, and the three-dimensional version in Section 3. After the buoyancy terms and the non-dimensional numbers in LBM are described in Section 4, the numerical results will be presented in Section 5. The conclusion in this study is described in the last section.

2. Binary fluids model

In modeling two-phase fluid, we use the binary fluids model proposed by Swift et al. [9], called BFSY model here, in which the repulsive interaction between two kinds of fluid component is associated with a free energy. The BFSY model consists of two sets of distribution functions and two kinds of the lattice Boltzmann equations with the lattice BGK collision operators [11],

$$f_a(t+\Delta t, \mathbf{r}+\mathbf{e}_a\Delta t) = f_a(t,\mathbf{r}) - \frac{1}{\tau_1}\big[f_a(t,\mathbf{r}) - f_a^{\mathrm{eq}}(t,\mathbf{r})\big], \tag{1}$$

$$g_a(t+\Delta t, \mathbf{r}+\mathbf{e}_a\Delta t) = g_a(t,\mathbf{r}) - \frac{1}{\tau_2}\big[g_a(t,\mathbf{r}) - g_a^{\mathrm{eq}}(t,\mathbf{r})\big], \tag{2}$$

where Δt is the time increment, $\mathbf{r}$ is the position vector of lattice site on the isotropic lattice, τ_1 and τ_2 are the relaxation time parameters, and $\mathbf{e}_a$ is the velocity vector of the fluid particles moving from a site $\mathbf{r}$ to its neighbors $\mathbf{r}+\mathbf{e}_a\Delta t$. The subscript a denotes the label to distinguish the fluid particles by their velocity vectors. In the two-dimensional hexagonal lattice with link length $= 1$ [2], it corresponds to the index i of the direction along link lines, $i = 1$ to 6 for moving particles with constant speed $c = 1/\Delta t$ and $i = 0$ for stationary particles. On the other hand, in the three-dimensional lattice consisting of two kind of the link lines with their length unity and $\sqrt{3}$ [12], the subscript a is replaced with two indices l and i to specify the kind of link lines and the direction, respectively, as described in Section 3. The functions f_a and g_a, respectively are related with the total number density of two fluid components A and B, $n = n_A + n_B$, and the number density difference between A and B, $\Delta n = n_A - n_B$. The above Eqs. (1) and (2) indicate that the distributions reach the states of local equilibrium f_a^{eq} and g_a^{eq} after time periods $\tau_1\Delta t$ and $\tau_2\Delta t$.

Hereafter, for the sake of convenience, a low-density and high-density phases, having the densities n_L and n_G, are referred to as gas and liquid respectively. The function Δn takes positive and negative values of identical magnitude for the liquid and the gas phase sides, respectively, representing two-phase distributions. Assumed that the liquid and gas phases correspond to the fluids in an A-rich and B-rich regions, respectively, n and Δn can be defined by the following equations,

$$n = \frac{n_L + n_G}{2}, \tag{3}$$

$$\Delta n = n_L F + n_G(1-F) - n, \tag{4}$$

where $0 < F < 1$ is the volume ratio of liquid phase. The function Δn takes the same absolute value Δn_0 in the liquid ($F = 1$) and the gas ($F = 0$) phases,

$$\Delta n_0 = \frac{n_L - n_G}{2}. \tag{5}$$

The macroscopic variables, number density n, density difference function Δn and velocity of two-phase fluid $\mathbf{u}$ are given from the functions f_a and g_a,

$$n = \sum_a f_a, \tag{6}$$

$$\Delta n = \sum_a g_a, \tag{7}$$

$$n\mathbf{u} = \sum_a f_a \mathbf{e}_a. \tag{8}$$

These quantities can be conserved locally at each lattice site in the collision step, because the following relations are constrained in the equilibrium state,

$$n = \sum_a f_a^{\mathrm{eq}}, \tag{9}$$

$$\Delta n = \sum_a g_a^{\mathrm{eq}}, \tag{10}$$

$$n\mathbf{u} = \sum_a f_a^{\mathrm{eq}} \mathbf{e}_a. \tag{11}$$

In order to describe the thermodynamic behavior of binary fluids system appropriately, the BFSY model incorporates the free energy that represents the repulsive interaction between fluid particles, which is related with the pressure tensor $P_{\alpha\beta}$ and the chemical potential difference $\Delta\mu$ between two phases,

$$\Delta\mu = -\frac{\lambda}{2}\frac{\Delta n}{n} + \frac{T}{2}\ln\left(\frac{n+\Delta n}{n-\Delta n}\right) - \kappa\nabla^2(\Delta n), \tag{12}$$

$$P_{\alpha\beta} = p\delta_{\alpha\beta} + \kappa\left(\frac{\partial n}{\partial r_\alpha}\frac{\partial n}{\partial r_\beta} + \frac{\partial \Delta n}{\partial r_\alpha}\frac{\partial \Delta n}{\partial r_\beta}\right), \tag{13}$$

where the Greek subscripts are Cartesian coordinate indices, $\delta_{\alpha\beta}$ the sign of Kronecker's delta, and

$$p = nT - \kappa\left[n\nabla^2 n + \Delta n\nabla^2(\Delta n)\right] - \frac{\kappa}{2}\left(|\nabla n|^2 + |\nabla \Delta n|^2\right). \tag{14}$$

In the above equations, λ represents the strength of interaction, T is the temperature of fluid, and κ is the control parameter of surface tension. As a result, two-phase separation is caused when T, a constant for whole flow field, is lower than the critical temperature $T_c = \lambda/2$.

The macroscopic dynamics of binary fluids can be derived from the mesoscopic evolution equations (1) and (2) through the multi-scale expansion technique. The former is related with the continuum equation and the equation of fluid motion, while the latter leads to the convection–diffusion equation for the function Δn corresponding to the two-phase distribution.

3. 3D binary fluids model

We developed the three-dimensional version based on the two-dimensional BFSY model. In the isotropic discretization of space and particle velocity, this model uses the same cubic lattice unit as the 15-velocity model (3D15V model) proposed by Chen et al. [12]. The subscript a in Eqs. (1) and (2) is replaced with two indices, l and i. l is the identification index of two kinds of the lattice links with their length unity and $\sqrt{3}$, while i is the index of the direction along lattice lines, $i = 1$ to 6 for $l = 1$, $i = 1$ to 8 for $l = 2$. $l = 0$ is assigned to stationary particles. The equilibrium distributions $f_{l,i}^{\mathrm{eq}}$ are represented on the limit of low Mach number by,

$$f_{l,i}^{\mathrm{eq}} = n\left[A_l + B_l\frac{(\mathbf{e}_{l,i}\cdot\mathbf{u})}{c^2} + C_l\frac{(\mathbf{e}_{l,i}\cdot\mathbf{u})^2}{c^4} + D_l\frac{(\mathbf{u}\cdot\mathbf{u})}{c^2}\right] + G_{\alpha\beta}^{(l)}\mathbf{e}_{l,i,\alpha}\mathbf{e}_{l,i,\beta}, \tag{15}$$

$$f_0^{\mathrm{eq}} = n\left[A_0 + D_0\frac{(\mathbf{u}\cdot\mathbf{u})}{c^2}\right], \tag{16}$$

where $c\Delta t = 1$, and the particles moves with the speeds $2c$ and $\sqrt{3}c$ on two link lines $l = 1$ and 2, respectively.

The dimensionless parameters A_l, B_l, C_l, and D_l are determined under some constraints to derive the Navier–Stokes equations from Eq. (1). As for A_l ($l = 0, 1, 2$), the following equations are given,

$$A_l = \frac{s_l}{8(s_1+s_2)c^2}\left[T - \kappa\left(\frac{\Delta n}{n}\nabla^2\Delta n + \nabla^2 n\right)\right], \tag{17}$$

$$A_0 = 1 - 6A_1 - 8A_2, \tag{18}$$

where s_l ($l = 0, 1, 2$) denotes the ratio of number density of particles in stationary equilibrium state, which determines the temperature T,

$$T = \frac{8(s_1+s_2)}{s_0+6s_1+8s_2}c^2. \tag{19}$$

The fluid in 3D15V model possesses the kinetic viscosity ν,

$$\nu = 4B_2(2\tau_1 - 1)c^2\Delta t. \tag{20}$$

The parameters in Eqs. (15) and (16) can be determined by the constraints to derive the Navier–Stokes equations from Eqs. (1). In this study,

$$B_1 = \tfrac{1}{12}, \quad B_2 = \tfrac{1}{24},$$
$$C_1 = \tfrac{1}{32}, \quad C_2 = \tfrac{1}{16},$$
$$D_0 = -\tfrac{7}{24}, \quad D_1 = -\tfrac{1}{48}, \quad D_2 = -\tfrac{1}{24}.$$

The tensor $G^{(l)}_{\alpha\beta}$ which yields the surface tension is defined as,

$$G^{(l)}_{\alpha\beta} = \frac{\kappa}{c^4}\left[E_l\left(\frac{\partial n}{\partial r_\alpha}\frac{\partial n}{\partial r_\beta} + \frac{\partial \Delta n}{\partial r_\alpha}\frac{\partial \Delta n}{\partial r_\beta}\right) + F_l(|\nabla n|^2 + |\nabla \Delta n|^2)\delta_{\alpha\beta}\right]. \tag{21}$$

E_l and F_l are the parameters determined by the constraints of the mass conservation in collision step (Eq. (9)) and the derivation of the pressure tensor $P_{\alpha\beta}$ (13),

$$\sum_{l,i} G^{(l)}_{\alpha\beta} e_{li\alpha} e_{li\beta} = 0, \tag{22}$$

$$\sum_{l,i} (nA_l + G^{(l)}_{\gamma\delta} e_{li\gamma} e_{li\delta}) e_{li\alpha} e_{li\beta} = P_{\alpha\beta}. \tag{23}$$

Calculating the summation of even-order velocity momentum on the spatial isotropy [12], the following results can be obtained.

$$E_1 = -F_1 = \frac{1}{32}, \quad E_2 = \frac{1}{16}, \quad F_2 = 0. \tag{24}$$

The equilibrium distributions in the binary fluids model, (15) and (16), correspond to those in the single phase fluid model exactly when the gradients of n and Δn vanish.

The another equilibrium distributions for Δn, $g^{\mathrm{eq}}_{l,i}$, are computed according to the following equations.

$$g^{\mathrm{eq}}_{l,i} = B_l\frac{\Gamma\Delta\mu}{c^2} + \Delta n\left[B_l\frac{(\mathbf{e}_{l,i}\cdot\mathbf{u})}{c^2} + C_l\frac{(\mathbf{e}_{l,i}\cdot\mathbf{u})^2}{c^4} + D_l\frac{(\mathbf{u}\cdot\mathbf{u})}{c^2}\right], \tag{25}$$

$$g^{\mathrm{eq}}_0 = \Delta n - \frac{\Gamma\Delta\mu}{c^2}\left(\sum_{l,i} B_l\right) + \Delta n D_0\frac{(\mathbf{u}\cdot\mathbf{u})}{c^2}, \tag{26}$$

where the parameter Γ represents the mobility. Because of $\sum_a (g_a - g^{\mathrm{eq}}_a)\mathbf{e}_a \neq 0$, the evolution equation in the BFSY model (2) includes the macroscopic diffusive effect of density difference function Δn, even though it is conserved locally at each lattice site in the collision. In this study, we adjust Γ to the suitable value to retain the initial volume of gas phase in the simulation of two-phase fluid motions without diffusion through some test runs.

4. Introduction of buoyancy effect

In this study, we introduce the buoyancy terms δf_a and δg_a to the lattice Boltzmann equations (1) and (2) in order to consider the effect due to the density difference between liquid and gas phases $\Delta n^* = 2\Delta n_0 = n_L - n_G$ under gravity. These terms are available only in the low density phase where the function Δn is negative, and satisfies the constraints of the net varieties of total number density and total momentum of particles as follows.

$$\sum_a \delta f_a = 0, \tag{27}$$

$$\sum_a \delta f_a \mathbf{e}_a = -\Delta n^* \mathbf{g}\Delta t. \tag{28}$$

The effect of buoyancy increases the number density distributions f_a in the opposite direction to the gravity g according to its magnitude $|g|$ and Δn^*, decreasing those in the gravity direction. On the other hand, the number density difference distributions g_a in the gravity direction increase, because the gas phase corresponds to the negative region of Δn. Then, the following relation is satisfied.

$$\delta g_a = -\delta f_a. \tag{29}$$

In two dimensions, the buoyancy term δf_i is added in the right hand side of Eq. (1) for the moving particles [13],

$$\delta f_i = \frac{\Delta n^*}{4}\frac{e_{i,y}}{|e_{i,y}|}\frac{|g|\Delta t}{c} \quad (i = 1, \ldots, 6), \tag{30}$$

where $e_{i,y}$ is the y-direction component of particle velocity in ith direction (see Fig. 1). In three dimensions,

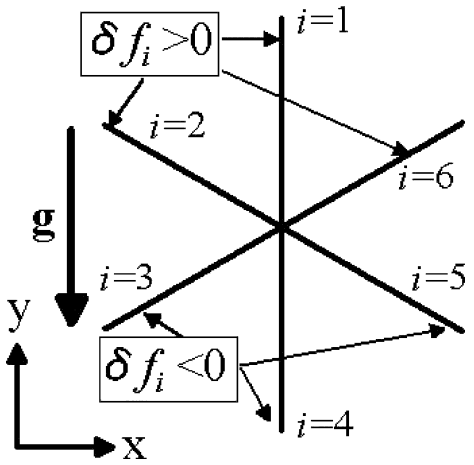

Fig. 1. The buoyancy terms δf_i in case of hexagonal lattice.

we use the following Eq. (31) to determine the buoyancy terms in the 15 directions of particle velocity simply,

$$\delta f_{l,i} = -\frac{\Delta n^*}{nT}(\mathbf{e}_{l,i} - \mathbf{u}) \cdot \mathbf{g} \Delta t f_{l,i}^{\mathrm{eq}}, \tag{31}$$

with $f_{l,i}^{\mathrm{eq}}$ excluding the gradient terms of n and Δn. The expression of the three-dimensional buoyancy term is different from the two-dimensional one, but both of the terms are quite equivalent in the macroscopic effect because these satisfy Eqs. (27) and (28).

The verification of non-dimensional numbers in LBM, that is, Eotvos and Morton numbers, Eo and M, are necessary to apply LBM to the two-phase flow analysis. In general, these numbers are defined with liquid viscosity ν_L, gas and liquid densities, ρ_G and ρ_L, surface tension σ, and characteristic length d as follows.

$$\mathrm{Eo} = \frac{|\mathbf{g}|(\rho_L - \rho_G)d^2}{\sigma}, \tag{32}$$

$$\mathrm{M} = \frac{|\mathbf{g}|\rho_L^2 \nu_L^4 (\rho_L - \rho_G)}{\sigma^3}. \tag{33}$$

In LBM, the surface tension σ is not given as a known macroscopic parameter, but results from the mesoscopic interaction between two kinds of fluid particles. Then, we determine the surface tension according to the Laplace's law which describes the balance of forces due to pressure difference and surface tension on interface. In two dimensions, it is represented by the equation,

$$\sigma = (P_{\mathrm{in}} - P_{\mathrm{out}})R, \tag{34}$$

where R is a curvature radius of interface, and P_{in} and P_{out} indicate the pressures inside and outside the gas phase fluid. Considering the buoyancy force according to Eq. (28), Eo and M in the BFSY model are defined as follows.

$$\mathrm{Eo} = \frac{2|\mathbf{g}|\Delta n^* d_B}{(P_{\mathrm{in}} - P_{\mathrm{out}})}, \tag{35}$$

$$\mathrm{M} = \frac{8|\mathbf{g}|\Delta n^* n_L^2}{d_B^3 (P_{\mathrm{in}} - P_{\mathrm{out}})^3} \left(\frac{2\tau_1 - 1}{8} \Delta t c^2 \right)^4. \tag{36}$$

In Eq. (35), the characteristic length corresponds to bubble diameter $d_B = 2R$. Setting Eo and M in the simulations, we use the value of σ working on the interface in stationary fluid without gravity.

5. Numerical results of bubble motions

5.1. Two-dimensional results in LBM and Volume Of Fluid method

Several numerical results of bubble motions are shown in comparison with those by the VOF method, which is one of the volume tracking method. The VOF method can simulate two-phase fluid motions by solving the Navier–Stokes equations and the convection equation for the volume ratio of liquid phase F,

$$\frac{\partial F}{\partial t} + \nabla \cdot (F\mathbf{u}) = 0. \tag{37}$$

In LBM, Eq. (37) can be derived from Eqs. (2) and (4), when the macroscopic diffusion term becomes negligible by adjusting the mobility Γ.

First of all, we simulate the two-dimensional single bubble motions in the stationary fluid. The density

Table 1
The parameters in the simulation of single bubble

Case	Eo	M	|g|
(a)	5	0.2267	7.750E−5
(b)	10	0.4535	1.550E−4
(c)	20	0.9070	3.100E−4
(d)	40	1.8134	6.200E−4
(e)	100	4.5350	1.550E−3

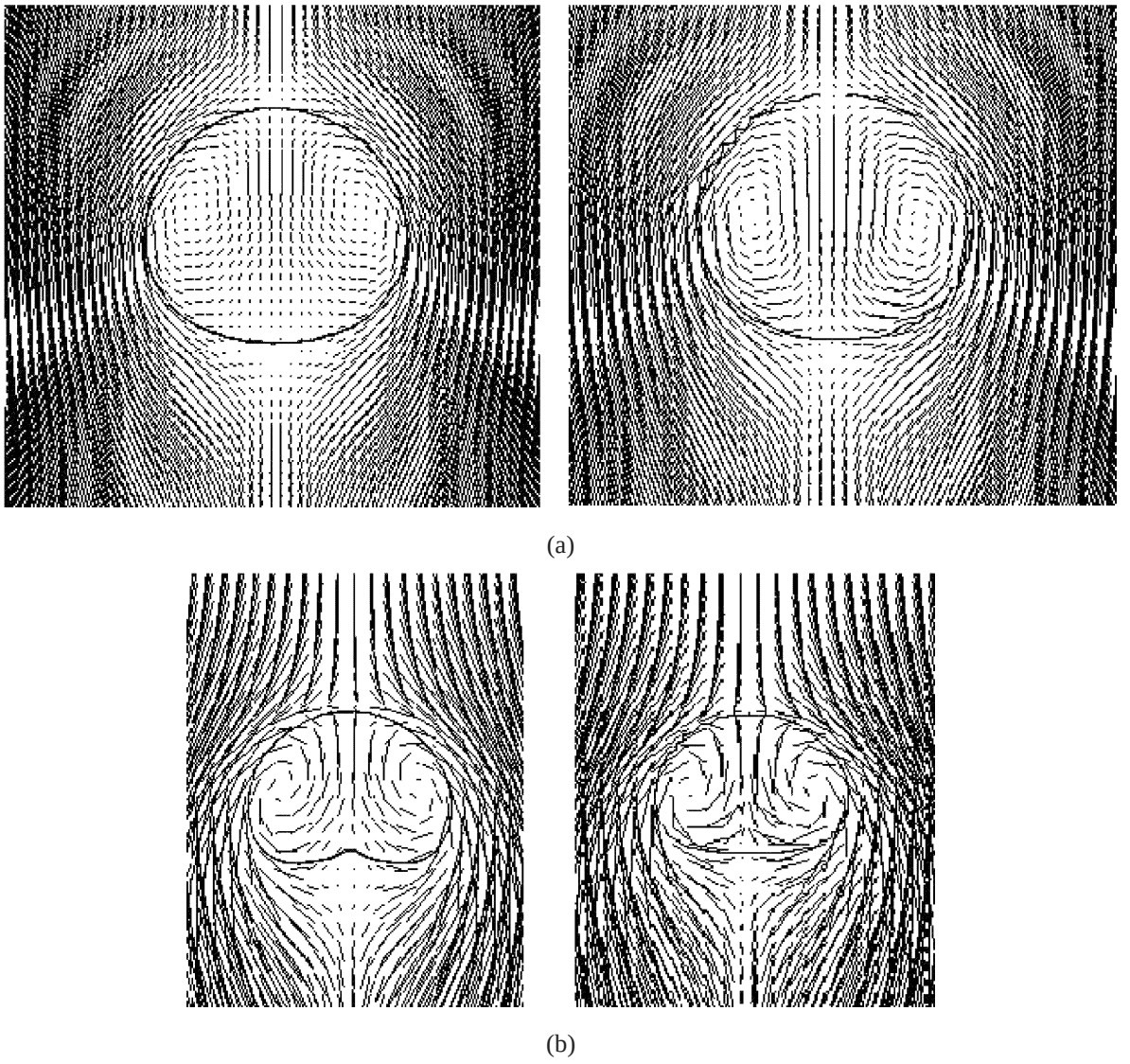

Fig. 2. The two-dimensional simulations of flow velocity field and interfacial profile of single bubble rising with terminal velocity in stationary fluid, for (a) Eo = 5, M = 0.2267, (b) Eo = 10, M = 0.4535, (c) Eo = 20, M = 0.9070, (d) Eo = 40, M = 1.8134, and (e) Eo = 100, M = 4.535. In each case, the left and right figures show the results by LBM and VOF method, respectively.

difference Δn^* is 0.84 for $n_L = 1.42$ and $n_G = 0.58$, corresponding to $n = 1$, $\kappa = 0.02$, $d_B = 20$, $\lambda = 1.1$, and $T = 0.5$, which result in $\sigma = 0.00521$, the relaxation time parameters $\tau_1 = \tau_2 = 1$, and $\Gamma = 0.05$. The flow field is surrounded with stationary walls, and initially a circular-shaped bubble is located in the lower region. This simulation was implemented with 80 lattice sites in x direction and 300 in y direction along the buoyancy force under several conditions of Eo and M, as shown in Table 1. The magnitude of gravity $|\mathbf{g}|$ was determined from the definition of Eo described in Eq. (35). The five figures in Fig. 2 show the flow velocity fields and the bubble shapes, simulated with LBM and VOF method. For each case,

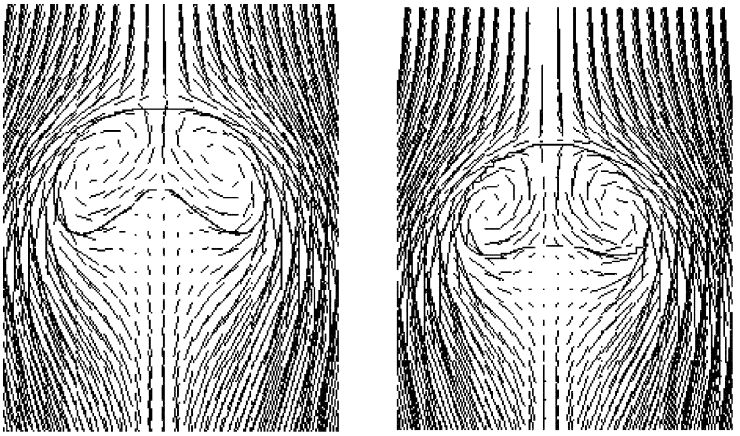

(c)

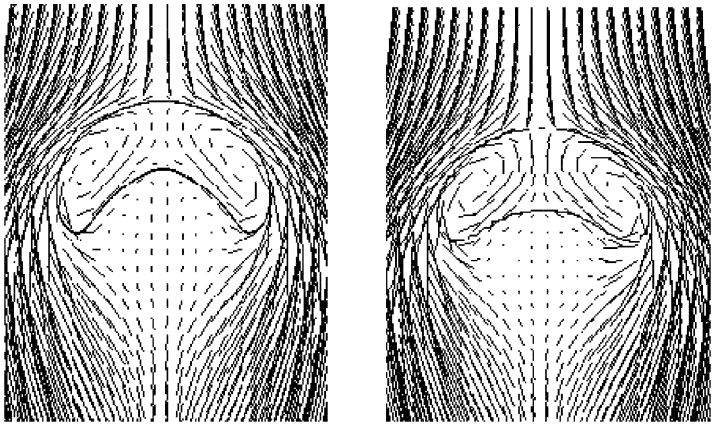

(d)

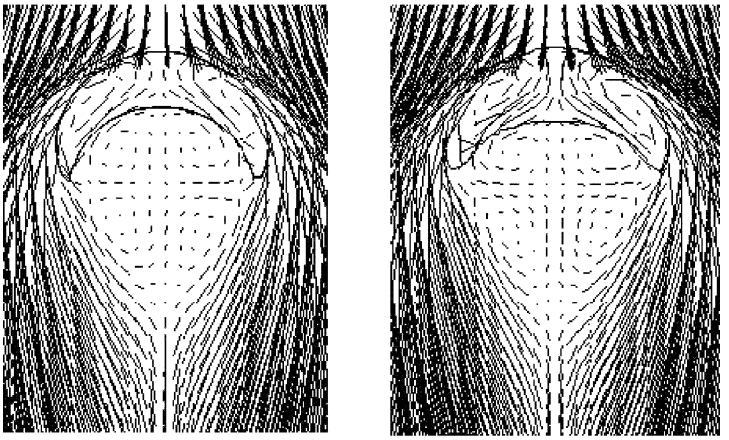

(e)

Fig. 2. (Continued.)

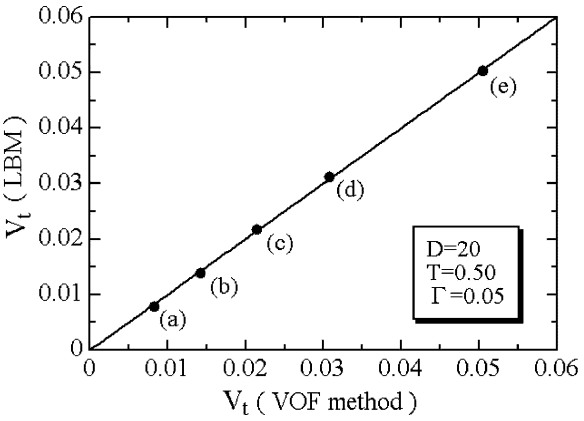

Fig. 3. The terminal rising velocities of single bubble for (a) Eo = 5, M = 0.2267, (b) Eo = 10, M = 0.4535, (c) Eo = 20, M = 0.9070, (d) Eo = 40, M = 1.8134, and (e) Eo = 100, M = 4.535, obtained by LBM and VOF method.

the bubbles arise at constant velocities because of the balance between buoyancy and drag forces. In these figures, the interface indicates the position where the density difference function Δn becomes zero. In terms of the shapes of bubble and the wake, the results obtained by LBM are similar to those by VOF method qualitatively, except the degree of deformation. As for the terminal velocity of bubble V_t, good agreement was obtained between LBM and VOF results within several percent error, as shown in Fig. 3 and Table 2.

Table 2
The terminal velocity of single bubble V_t

Case	V_t (LBM)	V_t (VOF)	Error in LBM (%)
(a)	7.82E−3	8.28E−3	−5.6
(b)	1.38E−2	1.43E−2	−3.5
(c)	2.17E−2	2.15E−2	+0.9
(d)	3.11E−2	3.08E−2	+1.0
(e)	5.03E−2	5.05E−2	−0.4

Next is the numerical result of bubble motion in the uniform shear flow for Eo = 10 and M = 0.82 in a duct with the right side wall moving upward at constant speed $4V_t$. Initially, the circular bubble is placed near the left stationary wall. The ratio of bubble diameter $d_B = 12$ to the duct width is about 0.25. Fig. 4 shows that the bubbles slide to the center of duct as rising

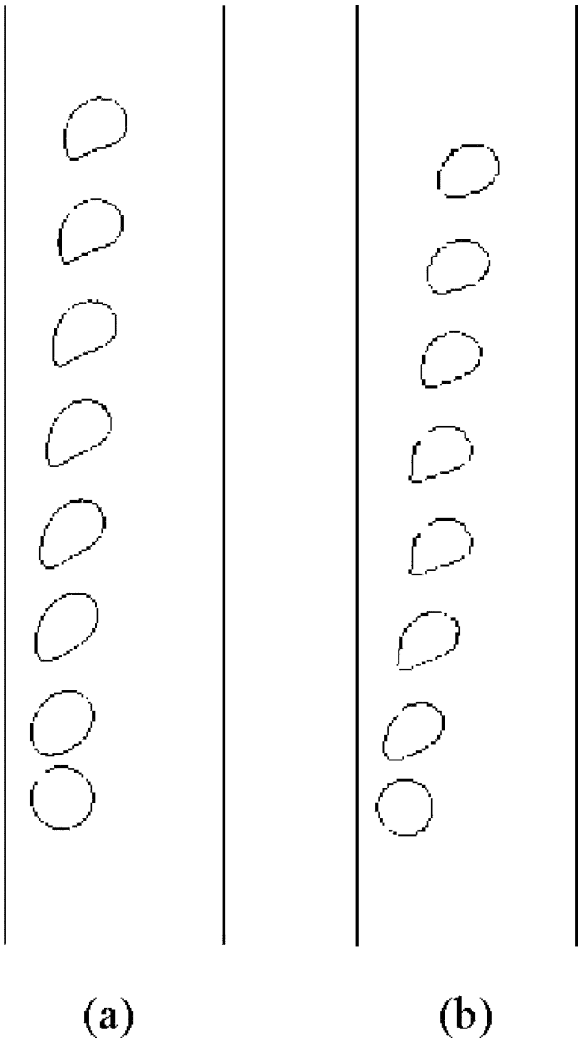

Fig. 4. The motion of single bubble in the uniform shear flow between the right wall moving upward and the left stationary wall for Eo = 10 and M = 0.82. The upper figures show the trajectories and the lower ones show the flow velocities, simulated by (a) LBM and (b) VOF method.

for both results by LBM and VOF method. Also, the flow velocity and the bubble shape are similar in both results, as shown in Fig. 5.

Third, we simulated the two-dimensional motions of two bubbles for Eo = 10 in a duct, where two stationary walls are placed 40 lattice sites away from the duct center. The fluid enters uniformly at the top boundary and leaves continuously at the bottom boundary so that the bubbles stay within the computed

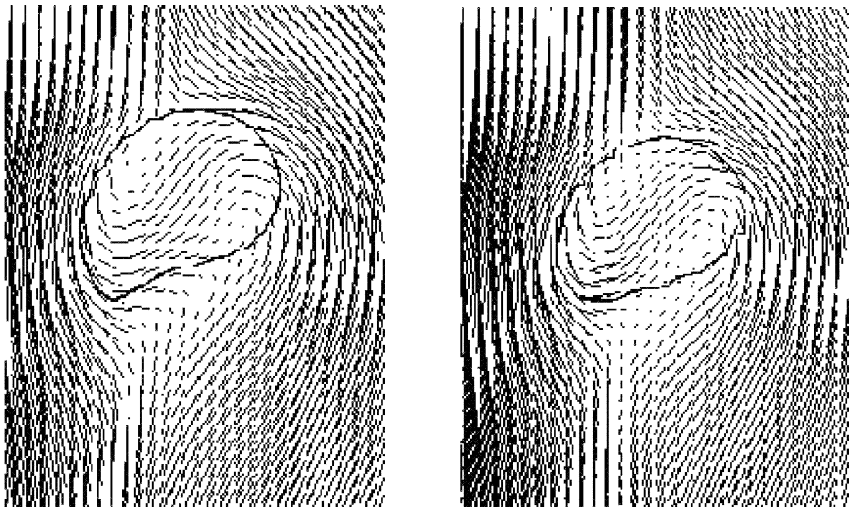

(a) (b)

Fig. 5. The flow velocity fields and the bubble shapes in the uniform shear flow.

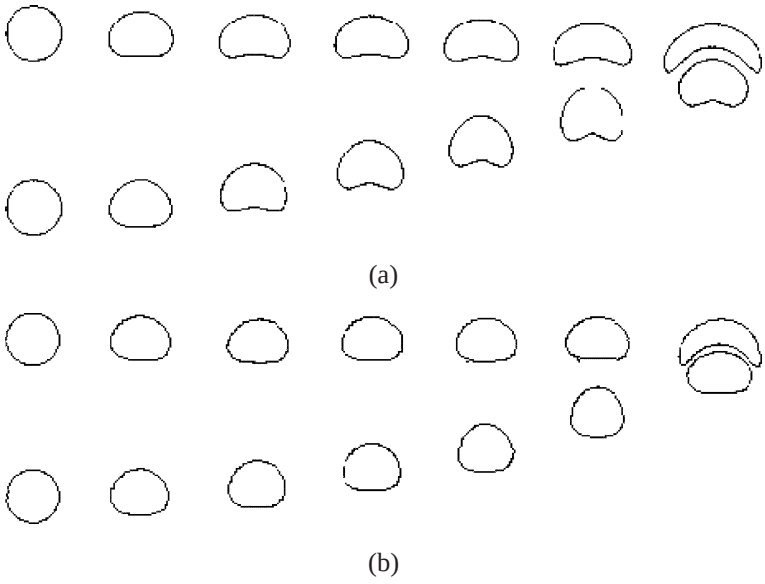

(a)

(b)

Fig. 6. The time series of snap shots of two bubbles for Eo = 10 in two dimensions. The figures (a) and (b) show the results simulated with LBM and VOF method, respectively, where the leftmost shots represent the initial condition of bubble diameter $d_B = 20$ distance between bubbles $L = 3d_B$ and the time interval corresponds to 2500 time steps in LBM.

flow field. Initially, two circular-shaped bubbles of $d_B = 20$ are placed three bubble diameter away from each other. Fig. 6 shows the time series of snap shots of the bubbles simulated with LBM and VOF method, respectively. The time interval of the shots corresponds to 2500 time steps in LBM. The upper bubble takes a shape of skirt as the lower one approaches due to the wake formation in both results by LBM and VOF method. In terms of the flow velocity and the dimensionless distance between

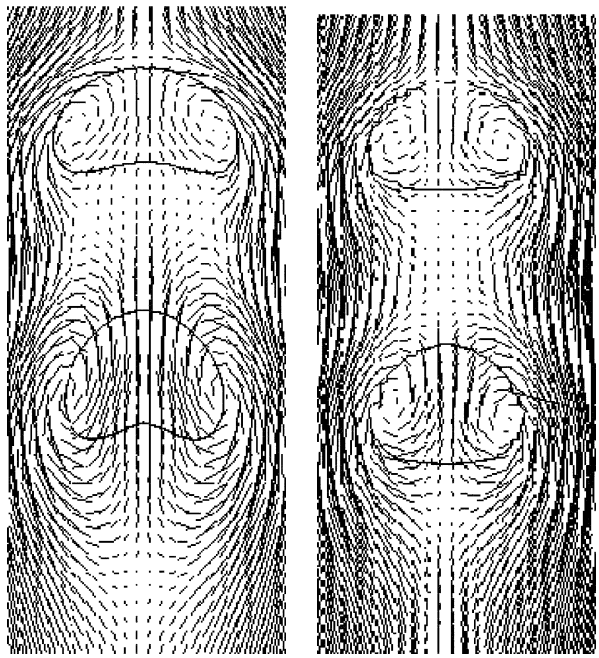

(a) (b)

Fig. 7. The flow velocity fields around two bubbles simulated with (a) LBM and (b) VOF method, at time corresponding to 10,000 time steps in LBM.

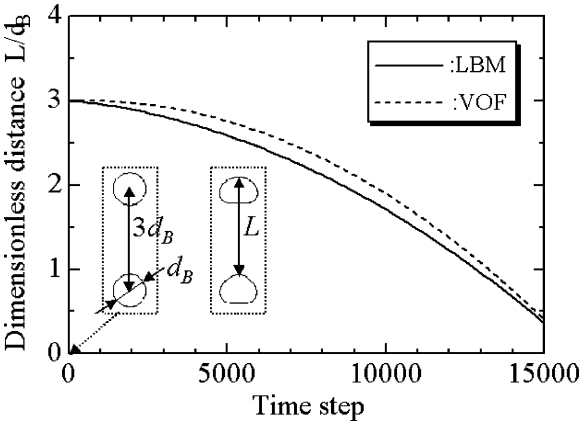

Fig. 8. The dimensionless distance between the top edges of bubbles with the initial diameter $d_B = 20$ for Eo $= 10$. The solid and the broken lines denote the results by LBM and VOF method, respectively.

bubbles shown in Figs. 7 and 8, these results agree well with each other.

In the LBM simulations, the thickness of the interface corresponds to the width of several lattice sites, where the value of Δn varies gradually from $-\Delta n_0$ in the gas phase to Δn_0 in the liquid phase. In this study, however, the buoyancy effect is added uniformly to the fluid particles in the domain where $\Delta n < 0$. That is the reason why the degree of the deformation of bubble in LBM is different from that in the VOF method which simulates the interface more sharply using the donor-acceptor scheme [10].

5.2. *Three-dimensional motions of two bubbles in LBM*

Following the successful simulation of 2D bubble motion, we attempted the simulation of three-dimensional motions of two bubbles for 2 cases. First, we simulated the coalescence of two bubbles with the diameter $d_B = 18$ in a stationary fluid without gravity, in order to check simply the surface tension effect in the 3D model. In this case, 51^3 lattice sites are gen-

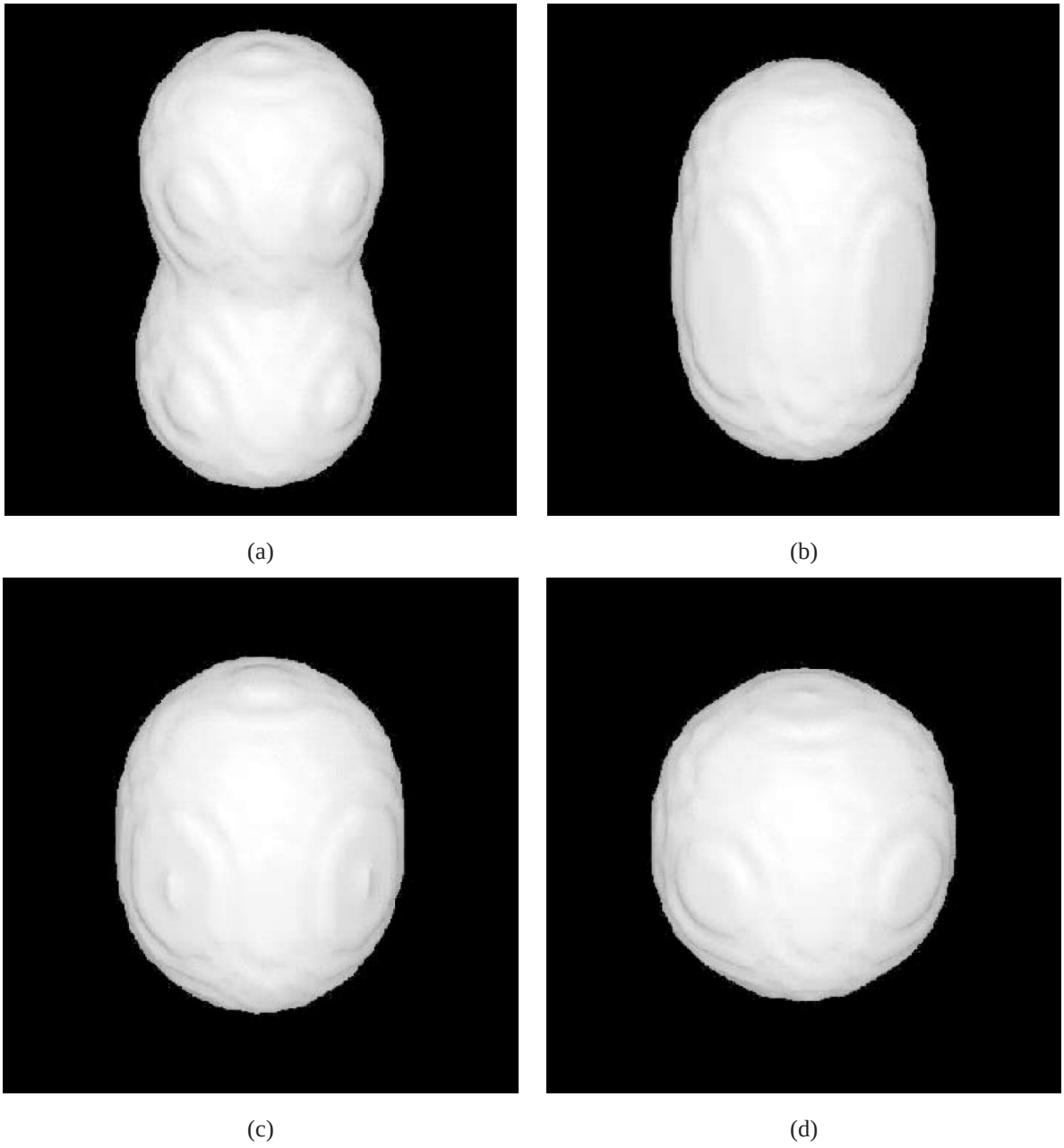

Fig. 9. The coalescence of two bubbles without gravity simulated by the three-dimensional BFSY model in LBM at time steps (a) 500, (b) 1000, (c) 1500, and (d) 2000.

erated in the cubic space surrounded with stationary walls, and the parameters are set as follows: $\kappa = 0.01$, $T = 0.5$, $n = 1$, $\Delta n_0 = 0.495$, $\lambda = 1.1$, and $\Gamma = 0.1$. As shown in Fig. 9, the spherical bubbles initially contacting to each other on their surfaces gradually fuse into a single bubble by the action of surface tension as time passes. This means that the surface tension term is modeled properly and isotropically.

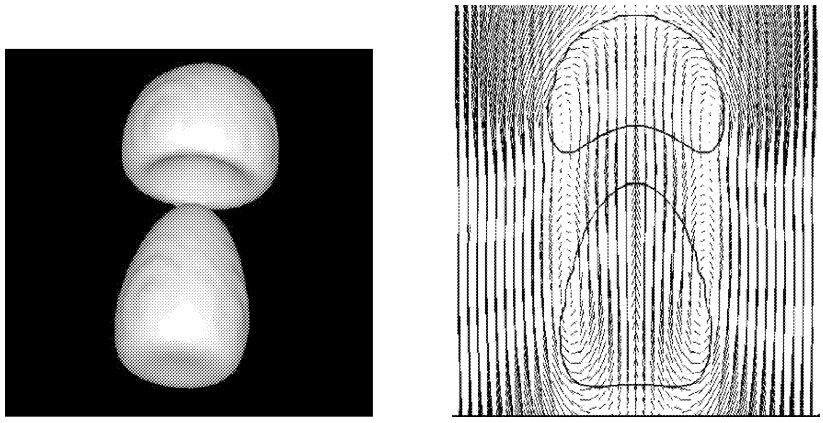

(a)

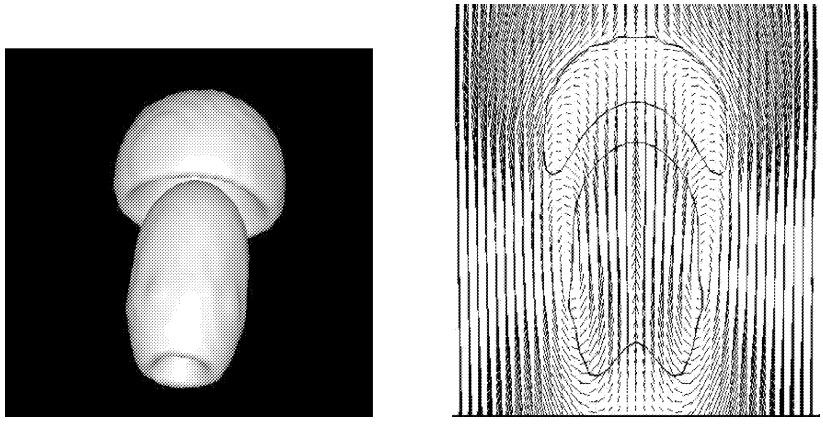

(b)

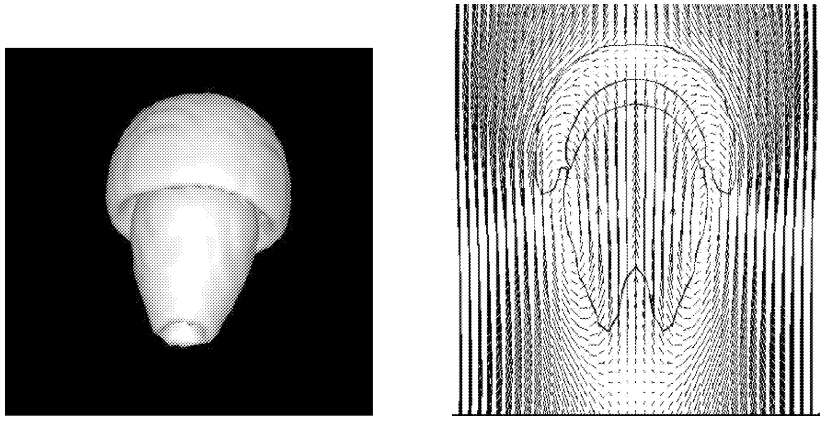

(c)

Fig. 10. The three-dimensional motion of two bubbles, which are rising in the circular tube under gravity for Eo = 50.1 and M = 1.5. The left figures show the bubble surfaces seen from bottom side, while the right ones show the bubble profile and the flow velocity on the vertical cross section through the center of tube, at (a) 500, (b) 1000, (c) 1500, (d) 2000, and (e) 2500 time steps.

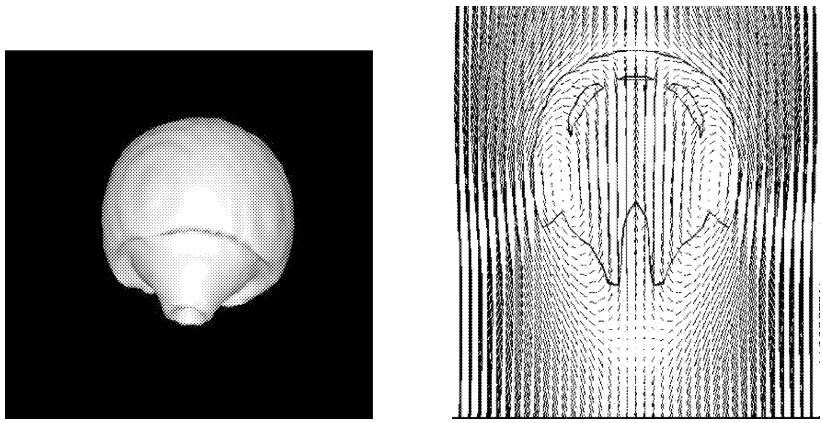

(d)

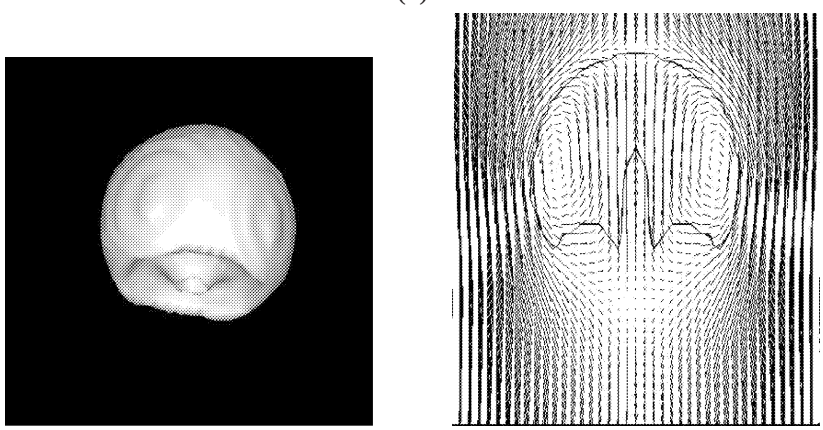

(e)

Fig. 10. (Continued.)

The second simulation depicts the three-dimensional motion of two bubbles with $d_B = 18$ under gravity, which are rising in the circular tube with diameter 48 in case of Eo = 50.1,M = 1.5 for $n = 1$, $\Delta n_0 = 0.495$, $\kappa = 0.01$, $\Gamma = 0.12$, $\lambda = 1.1$, $T = 0.5$, and $\nu_L = 0.1$. The flow field is discretized with 53, 53, and 75 lattice sites in x, y and z directions, and the fluid enters downward from the top boundary uniformly with the same velocity -0.022 as the tube wall. It is nearly equal to the rising velocity of bubbles and corresponds to the bubble Reynolds number $\mathrm{Re}_b = 4.0$. In the initial condition, the bubbles are initially placed away from each other by $1.4d_B$ along the center line of tube. In Fig. 10, the upper figures show the bubble surfaces seen from bottom side, while the lower ones show the bubble profile and the flow velocity on the vertical cross section through the center of tube. As seen in 2D simulation, the lower bubble approaches the upper one due to the wake formation, and they coalesce into a single bubble eventually. This means that 3D BFSY model is appropriately installed for the numerical simulation of bubble motions.

6. Concluding remarks

In the lattice Boltzmann method, we modeled the buoyancy effect and developed the three-dimensional

version of the binary fluids model applicable to two-phase fluid motions under gravity. The two-dimensional results agree well with those simulated by the Volume Of Fluid method. The three-dimensional simulations of two bubbles show that the surface tension works properly and that the model is capable of reproducing the process of two bubbles approaching due to the wake formation and coalescing into a single bubble. These results prove that the buoyancy effect and the 3D model proposed here are useful in simulating the two-phase fluid motions under gravity.

References

[1] G. McNamara, G. Zanetti, Phys. Rev. Lett. 61 (1988) 2332.
[2] U. Frisch, B. Hasslacher, Y. Pomeau, Phys. Rev. Lett. 56 (1986) 1505.
[3] U. Frisch, D. d'Humieres, B. Hasslacher, P. Lallemand, Y. Pomeau, J.P. Rivet, Complex Systems 1 (1987) 649.
[4] A.K. Gunstensen, H. Rothman, S. Zaleski, G. Zanetti, Phys. Rev. A 43 (1991) 4320.
[5] D. Grunau, S. Chen, K. Eggert, Phys. Fluids A 10 (1993) 2557.
[6] X.W. Shan, H.D. Chen, Phys. Rev. E 47 (1993) 1815.
[7] X.W. Shan, H.D. Chen, Phys. Rev. E 49 (1994) 2941.
[8] M.R. Swift, W.R. Osborn, J.M. Yeomans, Phys. Rev. Lett. 75 (1995) 830.
[9] M.R. Swift, E. Orlandini, W.R. Osborn, J.M. Yeomans, Phys. Rev. E 54 (1996) 5041.
[10] C.W. Hirt, B.D. Nichols, J. Comput. Phys. 39 (1981) 201.
[11] Y.H. Qian, D. d'Humieres, P. Lallemand, Europhys. Lett. 17 (1992) 479.
[12] S. Chen, Z. Wang, X. Shan, G.D. Doolen, J. Stat. Phys. 68 (1992) 379.
[13] D.R. Noble, S. Chen, J.G. Georgiadis, R.O. Buckius, Phys. Fluids 7 (1995) 203.